Inorganic Chemistry

Article

pubs.acs.org/IC

Dinuclear $[(V^{V}O(putrebactin))_2(\mu\text{-}OCH_3)_2]$ Formed in Solution as Established from LC-MS Measurements Using ^{50}V-Enriched V_2O_5

Cho Zin Soe,[†] Amalie A. H. Pakchung,[‡] and Rachel Codd*[,†]

[†]School of Medical Sciences (Pharmacology) and Bosch Institute and [‡]School of Chemistry, The University of Sydney, Sydney, New South Wales 2006, Australia

Supporting Information

ABSTRACT: Analysis of 1:1 solutions of V(V) and the macrocyclic dihydroxamic acid siderophore putrebactin (pbH_2) in 1:1 H_2O/CH_3OH using triple quadrupole liquid chromatography−mass spectrometry (LC-MS-QQQ) (pH ≈ 4) showed two well-resolved peaks ($t_R(1)$ 10.85 min; $t_R(2)$ 14.27 min) using simultaneous detection modes (absorbance, 450 nm; selective ion monitoring, m/z 437) characteristic of the previously identified oxidoV(V) complex $[V^{V}O(pb)]^+$ ($[M]^+$, m/z_{calc} 437.1). Peak 1 gave mass spectrometry (MS) signals consistent with $[V^{V}O(pb)]^+$, together with $[V^{V}O(pb)(OH)]$ and the dinuclear complexes $[(V^{V}O(pb))_2(\mu\text{-}OH)]^+$ and $[(V^{V}O(pb))_2(\mu\text{-}OH)_2]$. Peak 2 gave MS signals consistent with $[V^{V}O(pb)]^+$, together with $[V^{V}O(pb)(OCH_3)]$ and the dinuclear complexes $[(V^{V}O(pb))_2(\mu\text{-}OCH_3)]^+$ and $[(V^{V}O(pb))_2(\mu\text{-}OCH_3)_2]$. This analysis showed that two groups of $V(V)/pbH_2$ complexes with water- or methanol-derived ancillary ligands were resolved by liquid chromatography (LC). The detection of $[V^{V}O(pb)]^+$ in both peaks could be accounted for by its production from dissociation (peak 1: $[(V^{V}O(pb))_2(\mu\text{-}OH)]^+ \rightarrow [V^{V}O(pb)]^+ + [V^{V}O(pb)(OH)]$; peak 2: $[(V^{V}O(pb))_2(\mu\text{-}OCH_3)]^+ \rightarrow [V^{V}O(pb)]^+ + [V^{V}O(pb)(OCH_3)]$). The assignment of the signal at m/z_{obs} 959.2 (100%) as the dinuclear complex $[(V^{V}O(pb))_2(\mu\text{-}OCH_3)_2]$ ($[M + Na^+]^+$, m/z_{calc} 959.3) and not an ion cluster of mononuclear $[V^{V}O(pb)(OCH_3)]$ ($\{2[M] + Na^+\}^+$, m/z_{calc} 959.3) was made unequivocal by the use of ^{50}V-enriched V_2O_5, which gave a signal with an isotope pattern comprising the sum of the patterns of the three constituent $^{51}V-^{51}V$, $^{51}V-^{50}V$, and $^{50}V-^{50}V$ species. Coordination of methoxide was confirmed upon the replacement of CH_3OH with CD_3OD, which generated $[(V^{V}O(pb))_2(\mu\text{-}OCD_3)_2]$ ($[M + Na^+]^+$, m/z_{calc} 965.3, m/z_{obs} 965.3). Analysis of 1:1 solutions of Mo(VI) and pbH_2 showed a single peak in the LC (t_R 16.04 min), which gave MS signals that were characterized as mononuclear $[Mo^{VI}(O)_2(pb)]$ ($[M + Na^+]^+$, m/z_{calc} 523.1, m/z_{obs} 523.1) and dinuclear $[(Mo^{VI}O(pb))_2(\mu\text{-}O)_2]$ ($[M + Na^+]^+$, m/z_{calc} 1019.1, m/z_{obs} 1019.2). The steric and electronic effects of the *cis*-dioxido group(s) in $[Mo^{VI}(O)_2(pb)]$ mitigated coordination of solvent-derived ancillary ligands. The work highlights the value of using isotopically enriched metal ion sources and deuterated solvents to deconvolute metal/siderophore solution speciation. The results have relevance for an improved understanding of the coordination chemistry of pbH_2 and other marine siderophores in V(V)- and Mo(VI)-rich surface ocean waters.

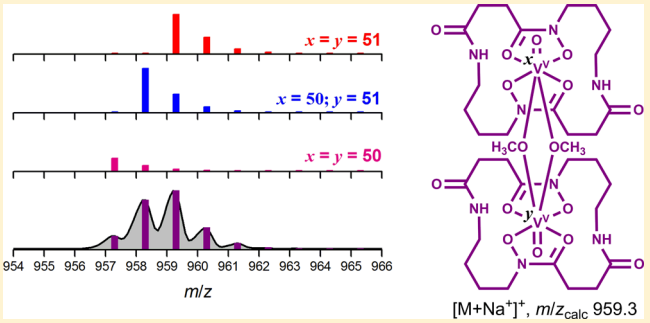

INTRODUCTION

Bacteria produce a class of high-affinity Fe(III) ligands known as siderophores that function to provide relatively insoluble Fe(III) in a more soluble form.[1−6] Uptake of the Fe(III)/siderophore complex is mediated by cell-surface receptors, with Fe(III) ultimately supplied to the bacterial cytoplasm as an element essential for growth.[7−9] Hydroxamic acids feature as one of the dominant functional groups of siderophores,[10,11] as present in the macrocyclic siderophore putrebactin (pbH_2, Scheme 1, **1**), which was first isolated from *Shewanella putrefaciens*.[12] The stoichiometry of $Fe(III)/pbH_2$ complexes is pH-dependent, with the 2:3 complex $[Fe_2(pb)_3]$ dominant at pH 7, and the 1:1 complex $[Fe(pb)]^+$ dominant under acidic conditions.[12−14] Although siderophores have been evolved for Fe(III) acquisition, these ligands form coordination complexes with a wide range of transition metal ions[15−19] and have applications as metal sequestering agents in medicine and the environment.[20−26] The speciation of siderophores produced by marine-dwelling bacteria with metal ions other than Fe(III) is relevant in ocean waters, which are abundant in Mo(VI) (∼100 nM) and V(V) (∼35 nM).[27−29] Previous work characterized the major complex formed in solution between V(V) and pbH_2 as $[V^{V}O(pb)]^+$ (Scheme 1, **2**), which gave a signal in the electrospray ionization-mass spectrum (ESI-MS) at m/z_{obs} 437.0 (100%) ($[M]^+$, m/z_{calc} 437.1).[30] The formation of $[V^{V}O(pb)]^+$ was invariant of pH value (from pH 2−7) and the $V(V)/pbH_2$ ratio. The same study used ESI-MS to characterize a series of dinuclear species formed between V(V) and the linear dihydroxamic acid suberodihydroxamic acid.[30]

Received: April 3, 2014
Published: May 16, 2014

   dx.doi.org/10.1021/ic500787v | Inorg. Chem. 2014, 53, 5852−5861

Scheme 1. Putrebactin (pbH_2, 1) and Its Complex with V(V) $[V^VO(pb)]^+$ (2) Characterized by Mass Spectrometry

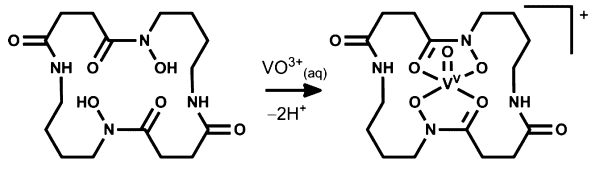

1
putrebactin (pbH_2)
$C_{16}H_{28}N_4O_6$
$[M+Na^+]^+$, m/z_{calc} 395.2

2
$[V^VO(pb)]^+$
$[C_{16}H_{26}N_4O_7V]^+$
$[M]^+$, m/z_{calc} 437.1

While the geometric constraints of macrocyclic pbH_2 might be thought to mitigate the formation of dinuclear V(V)/pbH_2 complexes, the presence or absence of such species remained unproven. The signal at m/z_{obs} 437.0 ascribed to $[V^VO(pb)]^+$ could be ascribable to the double-charged dinuclear complex $[(V^VO(pb))_2]^{2+}$. Since the isotopic distribution of V is dominated by ^{51}V (^{51}V, 99.75%; ^{50}V, 0.25%), the V-derived component of the MS isotope pattern for $[V^VO(pb)]^+$ and $[(V^VO(pb))_2]^{2+}$ would not be distinguishable. The assignment of the MS signals from V(V)/pbH_2 solutions to single-charged mononuclear or double-charged dinuclear species would be made clear by the use of a ^{50}V-enriched V(V) source.

In this work, the speciation of the V(V)/pbH_2 system was examined using triple-quadrupole liquid chromatography−mass spectrometry (LC-MS-QQQ) using V_2O_5 or ^{50}V-enriched V_2O_5 as the V(V) source. The work characterized a series of mononuclear and dinuclear V(V)/pbH_2 species, with the assignment of the dinuclear species made unequivocal from the data from the ^{50}V-enriched V_2O_5 system. Mononuclear and dinuclear Mo(VI)/pbH_2 complexes were also identified. The characterization of these species within the experimental boundaries of LC-MS contributes to the understanding of the coordination chemistry of marine siderophores in V(V)- and Mo(VI)-rich waters.

RESULTS AND DISCUSSION

LC-MS Measurements from Solutions of V(V) and pbH_2: Opening Comments. Putrebactin was purified from 3 × 100 mL cultures of *S. putrefaciens* using a two-step procedure (XAD chromatography, Ni(II)-based immobilized metal ion affinity chromatography) to give a final yield of 5.6 mg L^{-1} (Supporting Information, Figure S1). Initial LC-MS studies of V(V)/pbH_2 speciation undertaken in this work used simultaneous detection modes of absorbance at 450 nm, which is the wavelength of maximum absorbance of V(V)/hydroxamic acid complexes,[30−32] and selected ion monitoring (SIM) at m/z 437, corresponding to $[V^VO(pb)]^+$ ($[M]^+$, m/z_{calc} 437.1).

The LC trace (abs 450 nm) from a solution of V(V) and pbH_2 in H_2O ($[V(V)]/[pbH_2]$ = 1:1; pH ≈ 4) showed a single peak at t_R 10.79 min (Figure 1a, black), while a solution in 1:1 H_2O/CH_3OH showed two well-resolved peaks in the LC at t_R 10.86 min (peak 1) and t_R 14.29 min (peak 2) (Figure 1b). While it was readily conceived that different V(V)/pbH_2 complexes with similar absorbance properties at 450 nm might be resolved by LC, it was more difficult to rationalize why these species would each be detectable using a SIM value at m/z 437 (Figure 1a,b, gray). The first posit for this observation was the presence of $[V^VO(pb)]^+$ ($[M]^+$, m/z_{calc} 437.1) and the dinuclear complex $[(V^VO(pb))_2]^{2+}$ ($[M]^+$, m/z_{calc} 437.1), which could have solvation properties that were

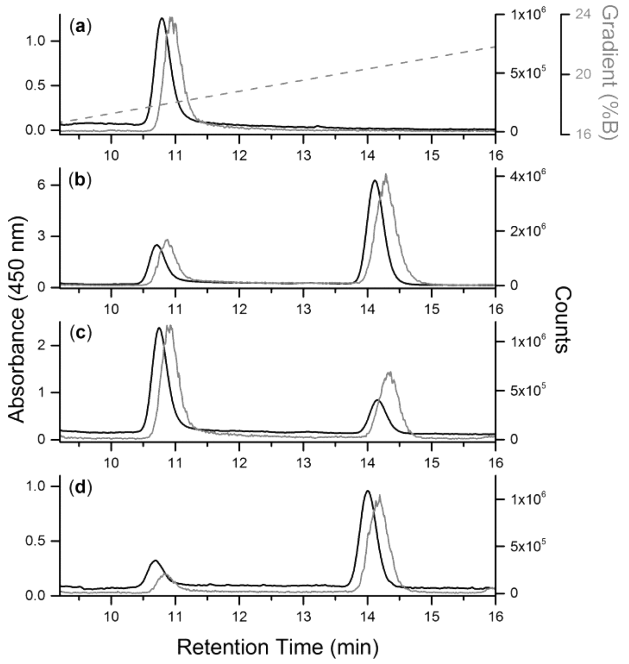

Figure 1. LC-MS traces from solutions ($[V(V)]/[pbH_2]$ = 1:1; pH ≈ 4) of (a) V(V)/pbH_2 in H_2O, (b) V(V)/pbH_2 in H_2O/CH_3OH, (c) $^{50,51}V(V)/pbH_2$ in H_2O/CH_3OH, or (d) V(V)/pbH_2 in CD_3OD. Detection used absorbance at 450 nm (black) or SIM counts at m/z 437 (gray). The gradient (gray, broken) in (a) was the same in (b)−(d).

sufficiently different to enable resolution by LC. The isotopic distribution of V would make the V-derived isotope patterns of $[V^VO(pb)]^+$ and $[(V^VO(pb))_2]^{2+}$ indistinguishable, which prompted further experiments using ^{50}V-enriched V_2O_5 as the V(V) source. The dinuclear complex $[(V^VO(pb))_2]^{2+}$ prepared from ^{50}V-enriched V_2O_5 would present as a distinct V-derived three-line isotope pattern with a line compression of 0.5 m/z units. The formation of double-charged complexes between Ga(III) or Fe(III) and linear dihydroxamic acids have been assigned from compressed isotope patterns.[33,34] The final condition examined in this work was the replacement of CH_3OH with CD_3OD as solvent. This was undertaken based on the occurrence of a single peak in the pure H_2O system and two peaks in the H_2O/CH_3OH system, which suggested that CH_3OH was modulating the V(V)/pbH_2 speciation. The solutions of $^{50,51}V(V)/pbH_2$ in H_2O/CH_3OH (Figure 1c) and V(V)/pbH_2 in H_2O/CD_3OD (Figure 1d) showed the resolution of two peaks in the LC, similar to the V(V)/pbH_2 in H_2O/CH_3OH system.

Assignment of Major Species from Solutions of V(V) and pbH_2. The MS trace from peak 1 (t_R(av) 10.85 min) across all the systems (V(V)/pbH_2 in H_2O, V(V)/pbH_2 in H_2O/CH_3OH, $^{50,51}V(V)/pbH_2$ in H_2O/CH_3OH, and V(V)/pbH_2 in H_2O/CD_3OD) showed the presence of $[V^VO(pb)]^+$ ($[M]^+$, m/z_{calc} 437.1) as the major (100%) species (Figure 2a,b,d) or as a dominant (66.5%) species (Figure 2f) (Table 1). Free pbH_2 ($[M + Na^+]^+$, m/z_{calc} 395.2, m/z_{obs} 395.2) was also present in peak 1 in relative concentrations ranging from 42.5 to 73.1% (Figure 2a,b,d) and at 100% in the V(V)/pbH_2 in H_2O/CD_3OD system (Figure 2f). The major signal at m/z_{obs} 477.1 in peak 1 (59−84%) formulated as $[V^VO(pb)(OH)]$ ($[M + Na^+]^+$, m/z_{calc} 477.1) (Chart 1, **3**) and has been previously observed from aged solutions of V(V) and pbH_2.[30]

dx.doi.org/10.1021/ic500787v | Inorg. Chem. 2014, 53, 5852−5861

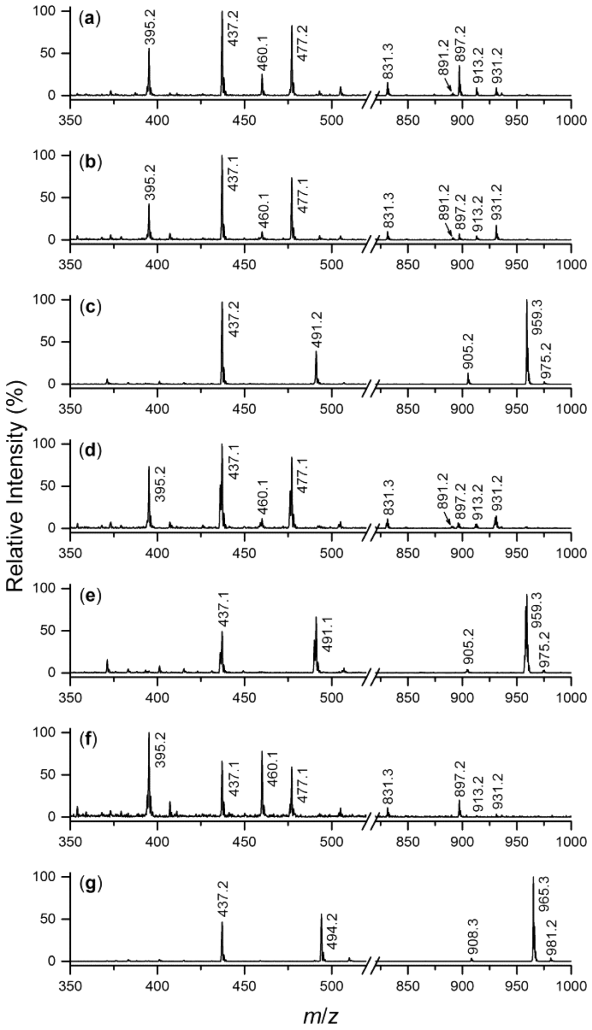

Figure 2. MS analysis (positive ion mode) of the LC peak from solutions ([V(V)]/[pbH$_2$] = 1:1; pH ≈ 4) of (a) V(V)/pbH$_2$ in H$_2$O at t_R 10.79 min; V(V)/pbH$_2$ in H$_2$O/CH$_3$OH at (b) t_R 10.86 min or (c) t_R 14.29 min; ^{50,51}V(V)/pbH$_2$ in H$_2$O/CH$_3$OH at (d) t_R 10.91 min or (e) t_R 14.33 min; and V(V)/pbH$_2$ in H$_2$O/CD$_3$OD at (f) t_R 10.84 min or (g) t_R 14.19 min.

The MS trace from peak 2 (t_R(av) 14.27 min), which was observed from V(V)/pbH$_2$ systems in H$_2$O/CH$_3$OH or H$_2$O/CD$_3$OD, showed no evidence of free pbH$_2$ (Figure 2c,e,g). A signal from the V(V)/pbH$_2$ in H$_2$O/CH$_3$OH system at m/z_{obs} 491.1 (39−66%) was consistent with the presence of [V^{V}O(pb)(OCH$_3$)] ([M + Na$^+$]$^+$, m/z_{calc} 491.1) (**4**).[30] In the V(V)/pbH$_2$ in H$_2$O/CD$_3$OD system, the signal at m/z_{obs} 494.2 (56%) correlated with [V^{V}O(pb)(OCD$_3$)] ([M + Na$^+$]$^+$, m/z_{calc} 494.2) (**5**), which supported the proposed coordination of the methoxide (**4**) or d_3-methoxide (**5**) group to the [V^{V}O(pb)]$^+$ core. The coordination of isopropoxide or methoxide to complexes with an oxidoV(V)/hydroxamic acid center have been shown in multiple X-ray crystallography studies.[31,35]

The major signal in peak 2 from the V(V)/pbH$_2$ in H$_2$O/CH$_3$OH system (Figure 2c,e) observed at m/z_{obs} 959.3 (93−100%) correlated with [(V^{V}O(pb))$_2$(μ-OCH$_3$)$_2$] ([M + Na$^+$]$^+$, m/z_{calc} 959.3) (**7**), which could form from the dimerization of [V^{V}O(pb)(OCH$_3$)] (**4**). In this structure, two methoxide ligands are proposed to coordinate in a μ-bridging fashion between the two oxidoV(V) centers, each of which feature a tetradentate pbH$_2$ coordinated as a dianion (pb(2−)). The μ-bridging coordination of two ethoxide ligands between two V(V) centers within a hexanuclear mixed ligand V(IV/V) complex has been shown from X-ray crystallography.[36] Low-intensity signals at m/z_{obs} 975.2 correlated with the potassium adduct of (**7**) ([M + K$^+$]$^+$, m/z_{calc} 975.3). The major MS signal (100%) present in the V(V)/pbH$_2$ in H$_2$O/CD$_3$OD system (m/z_{obs} 965.3) was consistent with [(V^{V}O(pb))$_2$(μ-OCD$_3$)$_2$] ([M + Na$^+$]$^+$, m/z_{calc} 965.3) (**8**), as a product of the dimerization of [V^{V}O(pb)(OCD$_3$)] (**5**).

Evidence of the formation of dinuclear complexes in peak 2 prompted a closer examination of peak 1. Low-intensity MS signals in peak 1 at m/z_{obs} 931.2 (4−17%) were consistent with the dimerization of [V^{V}O(pb)(OH)] (**3**) to give [(V^{V}O(pb))$_2$(μ-OH)$_2$] ([M + Na$^+$]$^+$, m/z_{calc} 931.2) (**6**).

Simulation of MS Isotope Patterns for Major Species from Solutions of V(V) and pbH$_2$. The experimental isotope pattern of the signal at m/z_{obs} 437.1 agreed with the simulation for [V^{V}O(pb)]$^+$ ([M]$^+$, m/z_{calc} 437.1) (Figure 3a). The replacement of V$_2$O$_5$ with ^{50}V-enriched V$_2$O$_5$ in the pbH$_2$ reaction system generated a signal centered at m/z_{obs} 437.1 ascribed to [^{50,51}V^{V}O(pb)]$^+$ ([M]$^+$, m/z_{calc} 437.1) (Figure 3b), with an isotope pattern consistent with the sum of the simulated isotope patterns of [^{51}V^{V}O(pb)]$^+$ ([M]$^+$, m/z_{calc} 437.1) (Figure 3c) and [^{50}V^{V}O(pb)]$^+$ ([M]$^+$, m/z_{calc} 436.1) (Figure 3d). The relative concentration of [^{51}V^{V}O(pb)]$^+$ and [^{50}V^{V}O(pb)]$^+$ was 90.2% and 50.7%, respectively (normalized for **2**: 64% and 36%), as prescribed by the 36% level of ^{50}V enrichment of V$_2$O$_5$. The isotope patterns of all species were simulated using the program ChemCalc.[37]

The signal observed at m/z_{obs} 959.2 in the ^{50,51}V(V)/pbH$_2$ in H$_2$O/CH$_3$OH system showed an isotope pattern (Figure 3e) that was consistent with the presence of dinuclear [(^{50,51}V^{V}O(pb))$_2$(μ-OCH$_3$)$_2$] ([M + Na$^+$]$^+$, m/z_{calc} 959.3) (**7**). The experimental isotope pattern for [(^{50,51}V^{V}O(pb))$_2$(μ-OCH$_3$)$_2$] presented as the sum of the simulated isotope patterns for [(^{51}V^{V}O(pb))$_2$(μ-OCH$_3$)$_2$] ([M + Na$^+$]$^+$, m/z_{calc} 959.3) (Figure 3f), [(^{51}V^{V}O(pb))(^{50}V^{V}O(pb))(μ-OCH$_3$)$_2$] ([M + Na$^+$]$^+$, m/z_{calc} 958.3) (Figure 3g), and [(^{50}V^{V}O(pb))$_2$(μ-OCH$_3$)$_2$] ([M + Na$^+$]$^+$, m/z_{calc} 957.3) (Figure 3h), present in relative concentrations of 66.8%, 75.1%, and 21.1%, respectively (normalized for [(^{50,51}V^{V}O(pb))$_2$(μ-OCH$_3$)$_2$]: 41.0%, 46.1% and 12.9%).

The simulated isotope patterns for [V^{V}O(pb)(OCH$_3$)] (Figure 4a) and [^{50,51}V^{V}O(pb)(OCH$_3$)] (Figure 4b) agreed closely with experiment ([M + Na$^+$]$^+$, m/z_{calc} 491.1). Coordination of methoxide was confirmed from the simulated and experimental isotope pattern of [V^{V}O(pb)(OCD$_3$)] (Figure 4c) ([M + Na$^+$]$^+$, m/z_{calc} 494.1). In the V(V)/pbH$_2$ in H$_2$O/CH$_3$OH or H$_2$O/CD$_3$OD system (Figure 4d,f, respectively), the respective coordination of two methoxide or d_3-methoxide units in dinuclear [(V^{V}O(pb))$_2$(μ-OCH$_3$)$_2$] (**7**) or [(V^{V}O(pb))$_2$(μ-OCD$_3$)$_2$] (**8**) was confirmed from the positive shift of m/z 6 units to the MS signal for the latter species.

The assignment of dinuclear [(V^{V}O(pb))$_2$(μ-OCH$_3$)$_2$] (**7**) was made unequivocal only through the use of ^{50}V-enriched V$_2$O$_5$ (Figures 3e and 4e). Although the signal at m/z_{obs} 959.2 observed from the V(V)/pbH$_2$ in H$_2$O/CH$_3$OH system prepared from standard V$_2$O$_5$ simulated as [(V^{V}O(pb))$_2$(μ-OCH$_3$)$_2$] ([M + Na$^+$]$^+$, m/z_{calc} 959.3) (Figure 4d), the signal was also consistent with the sodiated ion of a cluster of the mononuclear complex [V^{V}O(pb)(OCH$_3$)] (**4**) ({2[M] +

dx.doi.org/10.1021/ic500787v | Inorg. Chem. 2014, 53, 5852−5861

Table 1. LC-MS Data of Species Characterized from Solutions of V(V) or ^{50,51}V(V) and pbH_2 in H_2O, H_2O/CH_3OH, or H_2O/CD_3OD

assignment	no	m/z_{obs}	m/z_{calc}	ion	V^V H_2O	V^V H_2O/CH_3OH		$^{50,51}V^V$ H_2O/CH_3OH		V^V H_2O/CD_3OD	
					t_R (min)	t_R (min)		t_R (min)		t_R (min)	
					10.79	10.86	14.29	10.91	14.33	10.84	14.19
					Figure 2a	Figure 2b	Figure 2c	Figure 2d	Figure 2e	Figure 2f	Figure 2g
					RI (%)[a]	RI (%)[a]	RI (%)[a]	RI (%)[a]	RI (%)[a]	RI (%)[a]	RI (%)[a]
pbH_2	**1**	395.2	395.2	$[M + Na^+]^+$	55.9	42.4	0	73.1	0	100	0
$[V^VO(pb)]^+$	**2**	437.1	437.1	$[M]^+$	100	100	97.5	100	49.0	66.5	46.6
$\{[V^VO(pb)]^+ \cdot pbH^-\}$	**2a**	831.3	831.3	$[M + Na^+]^+$	15.4	9.9	0	11.1	0	11.2	0
$[V^VO(pb)(OH)]$	**3**	477.1	477.1	$[M + Na^+]^+$	82.8	73.7	0	84.1	0	59.3	0
$[V^VO(pb)(OCH_3)]$	**4**	491.2	491.1	$[M + Na^+]^+$	0	0	38.8	0	66.1	0	0
$[V^VO(pb)(OCD_3)]$	**5**	494.2	494.2	$[M + Na^+]^+$	0	0	0	0	0	0	56.2
$[(V^VO(pb))_2(\mu\text{-}OH)_2]$	**6**	931.2	931.2	$[M + Na^+]^+$	9.3	17.3	0	14.6	0	3.6	0
$[(V^VO(pb))_2(\mu\text{-}OCH_3)_2]$	**7**	959.2	959.3	$[M + Na^+]^+$	0	0	100	0	93.1	0	0
		975.2	975.3	$[M + K^+]^+$	0	0	2.9	0	3.3	0	0
$[(V^VO(pb))_2(\mu\text{-}OCD_3)_2]$	**8**	965.3	965.3	$[M + Na^+]^+$	0	0	0	0	0	0	100
		981.2	981.3	$[M + K^+]^+$	0	0	0	0	0	0	4.1
$[(V^VO(pb))_2(\mu\text{-}OH)]^+$	**9**	891.2	891.2	$[M]^+$	3.0	2.5	0	2.3	0	0	0
$[(V^VO(pb))_2(\mu\text{-}OCH_3)]^+$	**10**	905.2	905.3	$[M]^+$	0	0	13.1	0	3.8	0	0
$[(V^VO(pb))_2(\mu\text{-}OCD_3)]^+$	**11**	908.3	908.3	$[M]^+$	0	0	0	0	0	0	3.9
$[(V^VO(pb))_2(\mu\text{-}O)]$	**12**	913.2	913.2	$[M + Na^+]^+$	9.5	4.8	0	5.1	0	1.8	0
$[V^{IV}O(pb)]$	**13**	460.1	460.1	$[M + Na^+]^+$	25.3	9.7	0	11.4	0	78.1	0
$[(V^{IV}pb)_2(\mu\text{-}O)_2]$	**14**	897.2	897.2	$[M + Na^+]^+$	35.5	7.4	0	5.3	0	20.0	0

[a]RI, relative intensity.

$Na^+\}^+$, m/z_{calc} 959.3). Because of the dominance of the ^{51}V isotope (99.75%), the distinction between the m/z value and isotope pattern for mononuclear $[V^VO(pb)(OCH_3)]$ (**4**) ($\{2[M] + Na^+\}^+$, m/z_{calc} 959.3) or dinuclear $[(V^VO(pb))_2(\mu\text{-}OCH_3)_2]$ (**7**) ($[M + Na^+]^+$, m/z_{calc} 959.3) would be equivocal using V_2O_5. The distribution of ^{51}V–^{51}V, ^{51}V–^{50}V, and ^{50}V–^{50}V species demonstrates the presence of dinuclear $[(V^VO(pb))_2(\mu\text{-}OCH_3)_2]$ (**7**) as the species correctly assigned to the signal at m/z_{obs} 959.2 (Figure 3e–h).

Assignment of Other Species from Solutions of V(V) and pbH_2. The MS trace from peak 2 of the V(V)/pbH_2 in H_2O/CH_3OH system (Figure 2c) showed a minor signal (13.1%) at m/z_{obs} 905.2, which was consistent with the presence of $[(V^VO(pb))_2(\mu\text{-}OCH_3)]^+$ (**10**) ($[M]^+$, m/z_{calc} 905.3), featuring a single μ-bridging methoxide group. Signals ascribable to the related dinuclear complexes $[(V^VO(pb))_2(\mu\text{-}OH)]^+$ (**9**) ($[M]^+$, m/z_{calc} 891.2) and $[(V^VO(pb))_2(\mu\text{-}OCD_3)]^+$ (**11**) ($[M]^+$, m/z_{calc} 908.3) were present at low concentrations (<4%).

A minor MS signal at m/z_{obs} 913.1 in peak 1 correlated with $[(V^VO(pb))_2(\mu\text{-}O)]$ (**12**) ($[M + Na^+]^+$, m/z_{calc} 913.2). Signals at m/z_{obs} 460.1 and m/z_{obs} 897.2 were assigned as $[V^{IV}O(pb)]$ (**13**) ($[M + Na^+]^+$, m/z_{calc} 460.1) and $[(V^{IV}O(pb))_2]$ (**14**) ($[M + Na^+]^+$, m/z_{calc} 897.2), respectively. The V(V) to V(IV) reduction was a likely result of the MS process,[38,39] which is supported by earlier work that showed that aerobic solutions of V(IV) and pbH_2 were electron paramagnetic resonance silent.[30] The similarity of the MS traces from a solution of V(V)/pbH_2 or V(IV)/pbH_2 (Supporting Information, Figure S2) showed that the speciation was independent of the oxidation state of the source V. The signal at m/z_{obs} 913.1 was also consistent with its assignment as the potassium adduct of $[(V^{IV}O(pb))_2]$ (**14**) ($[M + K^+]^+$, m/z_{calc} 913.2), and it was not possible to unambiguously assign this minor signal to **12** or **14**.

The minor MS signal at m/z_{obs} 831.3 in peak 1 showed an isotope pattern in the ^{50,51}V(V)/pbH_2 system that was consistent with a mononuclear V species (Supporting Information, Figure S3). Despite the m/z value of this signal being in a region that could suggest its formulation as a dinuclear complex, the V-derived two-line isotope pattern in the ^{50}V-enriched V_2O_5 system supported its assignment as $\{[V^VO(pb)]^+ \cdot pbH^-\}$ ($[M + Na^+]^+$, m/z_{calc} 831.3, m/z_{obs} 831.3). The experimental MS data for all metal–ligand species assigned in this work showed excellent agreement with the simulated isotope pattern (Supporting Information, Figure S3).

LC-MS Measurements from Solutions of V(V) and pbH_2: Closing Comments. Analysis of the MS traces from peak 1 and peak 2 in the LC from solutions of V(V) and pbH_2 in H_2O or in H_2O/CH_3OH or H_2O/CD_3OD have shown that peak 1 contained $[V^VO(pb)]^+$ (**2**) in addition to a group of complexes with water-derived ancillary ligands $[V^VO(pb)(OH)]$ (**3**), $[(V^VO(pb))_2(\mu\text{-}OH)_2]$ (**6**), and $[(V^VO(pb))_2(\mu\text{-}OH)]^+$ (**9**), and that peak 2 contained $[V^VO(pb)]^+$ (**2**) in addition to a group of complexes with methanol-derived ancillary ligands $[V^VO(pb)(OCH_3)]$ (**4**), $[(V^VO(pb))_2(\mu\text{-}OCH_3)_2]$ (**7**), and $[(V^VO(pb))_2(\mu\text{-}OCH_3)]^+$ (**10**). The coordination of methoxide in (**4**), (**7**), and (**10**) was verified by the equivalent complexes formed from CD_3OD solutions, namely, complexes (**5**), (**8**), and (**11**). The dimerization of (**3**), (**4**), or (**5**) would form (**6**), (**7**), or (**8**), respectively. The reaction between (**2**) and mononuclear (**3**), (**4**), or (**5**) would form (**9**), (**10**), or (**11**), respectively (Scheme 2). The association of two monomers to form a given dinuclear complex implies that each type of dinuclear complex could also undergo dissociation to the constituent monomers. This provides a rationale for the detection by MS of $[V^VO(pb)]^+$ in peak 1 and peak 2, since it could form in peak 1 as a dissociation product of $[(V^VO(pb))_2(\mu\text{-}OH)]^+$ (**9**) → $[V^VO(pb)]^+$ (**2**) + $[V^VO(pb)(OH)]$ (**3**) and in peak 2 as a dissociation product of $[(V^VO(pb))_2(\mu\text{-}OCH_3)]^+$ (**10**) → $[V^VO(pb)]^+$ (**2**) + $[V^VO(pb)(OCH_3)]$ (**4**) (Scheme 2).

dx.doi.org/10.1021/ic500787v | Inorg. Chem. 2014, 53, 5852–5861

Chart 1. Species Characterized Using LC-MS from Solutions of V(V) or ^{50,51}V(V) and pbH$_2$ in H$_2$O, H$_2$O/CH$_3$OH, or H$_2$O/CD$_3$OD

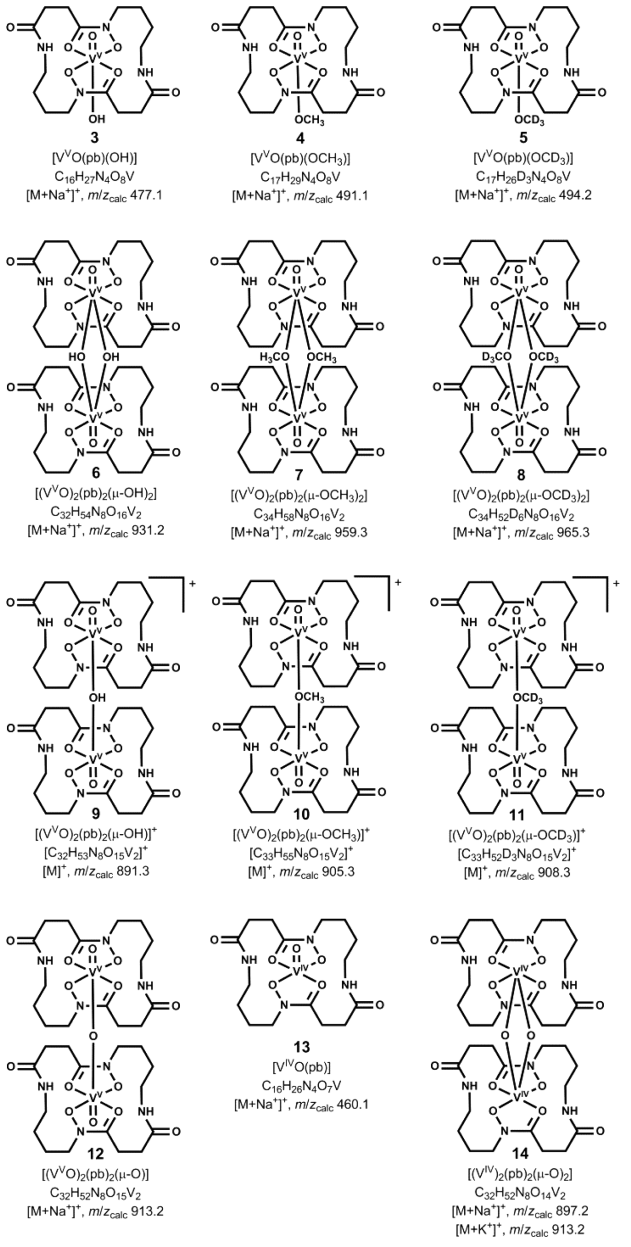

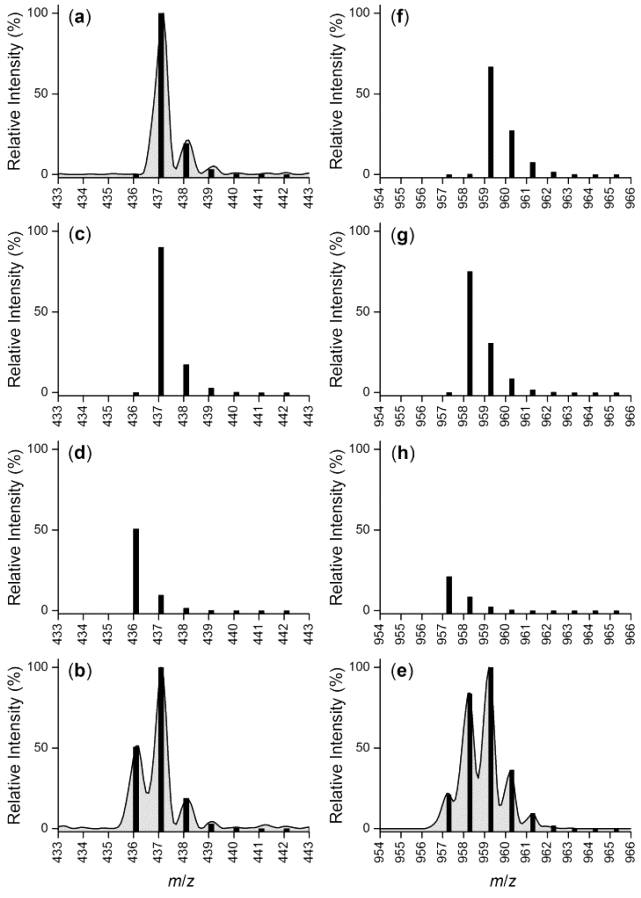

Figure 3. Experimental (Gaussian, gray) and simulated (black) MS data for (a) $[V^VO(pb)]^+$ ($[M]^+$, m/z_{calc} 437.1); (b) $[^{50,51}V^VO(pb)]^+$ ($[M]^+$, m/z_{calc} 437.1), comprising the sum of signals for (c) $[^{51}V^VO(pb)]^+$ ($[M]^+$, m/z_{calc} 437.1) and (d) $[^{50}V^VO(pb)]^+$ ($[M]^+$, m/z_{calc} 436.1); and (e) $[(^{50,51}V^VO(pb))_2(\mu\text{-}OCH_3)_2]$ ($[M + Na^+]^+$, m/z_{calc} 959.3), comprising the sum of signals for (f) $[(^{51}V^VO(pb))_2(\mu\text{-}OCH_3)_2]$ ($[M + Na^+]^+$, m/z_{calc} 959.3), (g) $[(^{51}V^VO(pb))(^{50}V^VO(pb))(\mu\text{-}OCH_3)_2]$ ($[M + Na^+]^+$, m/z_{calc} 958.3), and (h) $[(^{50}V^VO(pb))_2(\mu\text{-}OCH_3)_2]$ ($[M + Na^+]^+$, m/z_{calc} 957.3). The relative intensities of the signals in (c) and (d) (as summed in (b)); and of (f), (g), and (h) (as summed in (e)), is prescribed by the 36% level of ^{50}V enrichment of V_2O_5.

This proposed distribution of V(V)/pbH$_2$ species was consistent with the analysis of the LC-MS data using different SIM values for detection (Figure 5). Peak 1 was detected simultaneously using absorbance at 450 nm and a SIM value at m/z 931, as representative of water-based $[(V^VO(pb))_2(\mu\text{-}OH)_2]$ ($[M + Na^+]^+$, m/z_{calc} 931) (Figure 5a–d; this peak was better resolved in a repeat experiment of the V(V)/pbH$_2$ in H$_2$O/CD$_3$OD system). Peak 2 was detected simultaneously using absorbance at 450 nm and a SIM value at m/z 959, as representative of methanol-based $[(V^VO(pb))_2(\mu\text{-}OCH_3)_2]$ ($[M + Na^+]^+$, m/z_{calc} 959) (Figure 5f,g) or in the CD$_3$OD system at m/z 965, as representative of $[(V^VO(pb))_2(\mu\text{-}OCD_3)_2]$ ($[M + Na^+]^+$, m/z_{calc} 965.3) (Figure 5h). Peak 1 was not detected with the SIM value at m/z 959 (or 965) (Figure 5e–h), and peak 2 was not detected with the SIM value at m/z 931 (Figure 5b–d), showing a complete resolution between the water-based (**3**, **6**, **9**) and methanol-based (**4**, **7**, **10**) species. The trend in elution time (t_R water-based species < t_R methanol-based species) was consistent with measures of hydrophobicity of the respective solvents (water < methanol).

Despite the mild ESI conditions used in this work, it is possible that the formation of the dinuclear complexes was a result of the MS process itself.[38−41] ESI-MS measurements from a solution of V(V) and pbH$_2$ in H$_2$O/CH$_3$OH at t = 0, 2, 30, 60, 120, or 260 min (Supporting Information, Figure S4) showed that the water-based monomer $[V^VO(pb)(OH)]$ (**3**) was dominant (100%) at $t \leq 2$ min and that the methanol-based monomer $[V^VO(pb)(OCH_3)]$ (**4**) was dominant (100%) at $t \geq 30$ min. At the time points t = 60, 120, and 260 min, mononuclear $[V^VO(pb)(OCH_3)]$ (**4**) was present (100%) together with low levels (4%) of dinuclear $[(V^VO(pb))_2(\mu\text{-}OCH_3)_2]$ (**7**). At the time point t = 30 min, mononuclear $[V^VO(pb)(OCH_3)]$ (**4**) was present (100%) with no detectable dinuclear complex. This difference in the relative concentrations of mononuclear and dinuclear complexes indicated that

dx.doi.org/10.1021/ic500787v | Inorg. Chem. 2014, 53, 5852−5861

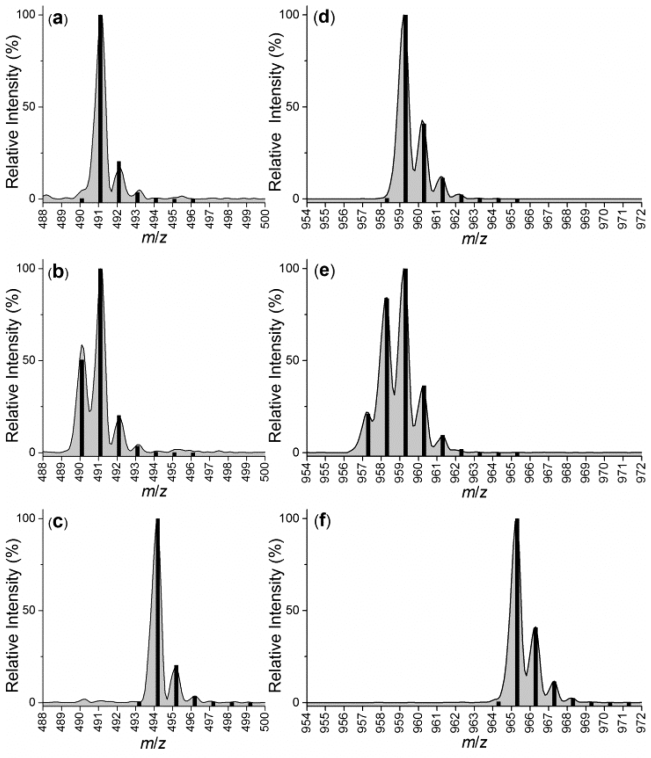

Figure 4. Experimental (Gaussian, gray) and simulated (black) MS data for (a) $[V^{V}O(pb)(OCH_3)]$ ($[M + Na^+]^+$, m/z_{calc} 491.1); (b) $[^{50,51}V^{V}O(pb)(OCH_3)]$ ($[M + Na^+]^+$, m/z_{calc} 491.1); (c) $[V^{V}O(pb)(OCD_3)]$ ($[M + Na^+]^+$, m/z_{calc} 494.2); (d) $[(V^{V}O)_2(pb)_2(OCH_3)_2]$ ($[M + Na^+]^+$, m/z_{calc} 959.3); (e) $[(^{50,51}V^{V}O)_2(pb)_2(OCH_3)_2]$ ($[M + Na^+]^+$, m/z_{calc} 959.3); or (f) $[(V^{V}O)_2(pb)_2(OCD_3)_2]$ ($[M + Na^+]^+$, m/z_{calc} 965.3).

the dinuclear complexes were not being produced solely as a result of the MS ionization process.

Seven-Coordinate Complexes from Solutions of V(V) and pbH_2. Complexes **6**, **7**, and **8** featured seven-coordinate oxido−V(V) centers, with each oxido−V(V) center coordinated to a doubly deprotonated tetradentate pbH_2 ligand and with metal−metal bridging provided from two μ-coordinated hydroxo (**6**), methoxide (**7**), or d_3-methoxide (**8**) ligands. Five- and six-coordinate oxido−V(V) species with hydroxamic acids have been extensively documented,[31,35,42−44] with seven-coordinate species occurring less frequently.

Supporting evidence for the formation of seven-coordinate oxido−V(V) species was provided from MS data from solutions of V(V) and the hexadentate trihydroxamic acid desferrioxamine B ($DFOBH_3$; Scheme 3, **15**). In aqueous solution, a signal at m/z_{obs} 625.3 (Figure 6) formulated as the seven-coordinate oxidoV(V) complex $[V^{V}O(DFOB)]$ ($[M + H^+]^+$, m/z_{calc} 625.3) (**16**), which was also present as the sodiated adduct ($[M + H^+]^+$, m/z_{calc} 647.3, m/z_{obs} 647.3) (Table 2). A signal at m/z_{obs} 608.3 formulated as the des-oxido−V(IV) species $[V^{IV}(DFOB)]^+$ ($[M^+]^+$, m/z_{calc} 608.3) (**17**). The formation of **17** is supported by the des-oxido−V(IV) complex with the siderophore enterobactin, which has been characterized by X-ray crystallography.[45] The V(V/IV) reduction could occur as a result of the MS process, as proposed similarly for the V(V/IV)/pbH_2 system. Previous potentiometric studies of complexes between V(V) and $DFOBH_3$ showed a 1:1 complex stoichiometry,[46] in accord with **16** and **17**. In methanol solutions, the relative intensity of the signal for **16** decreased with a concomitant increase in signals at m/z_{obs} 657.3 and 679.3, the latter of which formulated as the protonated and sodiated adducts of $[V^{V}O(DFOB)]\cdot CH_3OH$, respectively.

Scheme 2. Distribution of V(V)/pbH_2 Species Resolved by LC at t_R 10.85 min (2, 3, 6, 9) and t_R 14.27 min (2, 4, 7, 10)

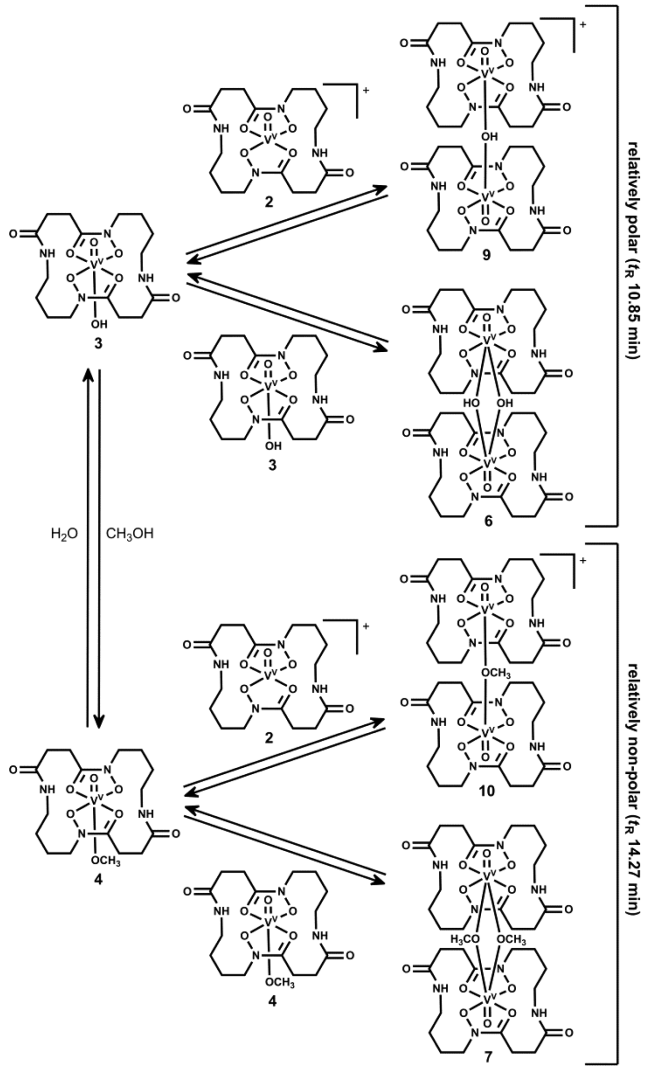

LC-MS Measurements from Solutions of Mo(VI) and pbH_2. Studies of the speciation between Mo(VI) and pbH_2 were of interest due to *S. putrefaciens* species being resident in marine environments, which are abundant in Mo(VI).[28,29,47] Peaks in the LC trace at t_R 15.91 min (H_2O) or t_R 16.11 min (H_2O/CH_3OH, H_2O/CD_3OD) from solutions of Mo(VI) and pbH_2 (Figure 7a−c) showed MS signals at m/z_{obs} 501.1, 523.1, and 1019.2 (Figure 7d−f, Table 3). The signal in the LC at t_R 12.7 min was not ascribable to a Mo-based species, due to the absence of the characteristic seven-line isotope pattern. The MS signals at m/z_{obs} 501.1 and 523.1 formulated as monomeric $[Mo^{VI}(O)_2(pb)]$ (**18**) present as protonated ($[M + H^+]^+$, m/z_{calc} 501.1) and sodiated ($[M + Na^+]^+$, m/z_{calc} 523.1) adducts. The MS signal at m/z_{obs} 1019.2 was consistent with the dinuclear species $[(Mo^{VI}O(pb))_2(\mu\text{-}O)_2]$ ($[M + Na^+]^+$, m/z_{calc} 1019.2) (**19**) (Chart 2). There was excellent agreement between the experimental and simulated isotope patterns for these species (Figure 7g,h). As distinct from the speciation of the V(V)/pbH_2 system, which differed between water and methanol solutions, the Mo(VI)/pbH_2 speciation was similar in

dx.doi.org/10.1021/ic500787v | Inorg. Chem. 2014, 53, 5852−5861

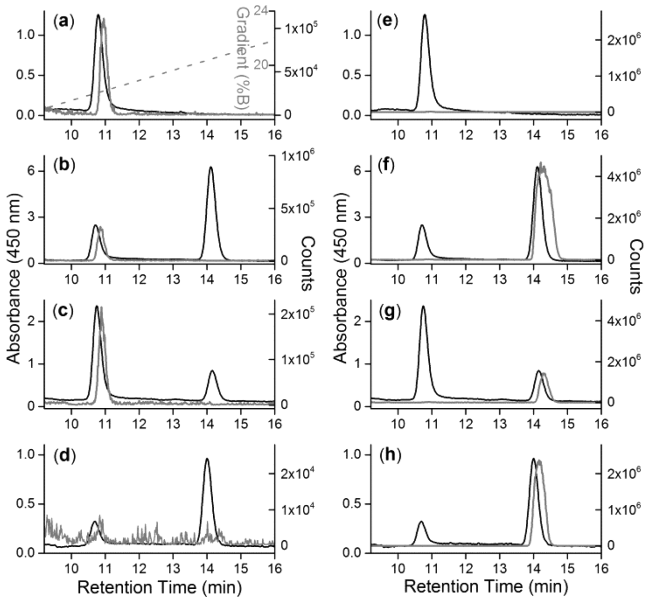

Figure 5. LC-MS traces from solutions ([V(V)]/[pbH$_2$] = 1:1; pH ≈ 4) of (a, e) V(V)/pbH$_2$ in H$_2$O; (b, f) V(V)/pbH$_2$ in H$_2$O/CH$_3$OH; (c, g) ^{50,51}V(V)/pbH$_2$ in H$_2$O/CH$_3$OH; or (d, h) V(V)/pbH$_2$ in CD$_3$OD. Detection used (a–h) absorbance at 450 nm (black); and SIM counts (gray) at: (a–d) *m*/*z* 931; (e–g) *m*/*z* 959; or (h) *m*/*z* 965. The gradient (gray, broken) in (a) was the same in (b)–(h).

Scheme 3. Species Characterized Using LC-MS From Solutions of V(V) and Desferrioxamine B (DFOBH$_3$) in H$_2$O or H$_2$O/CH$_3$OH

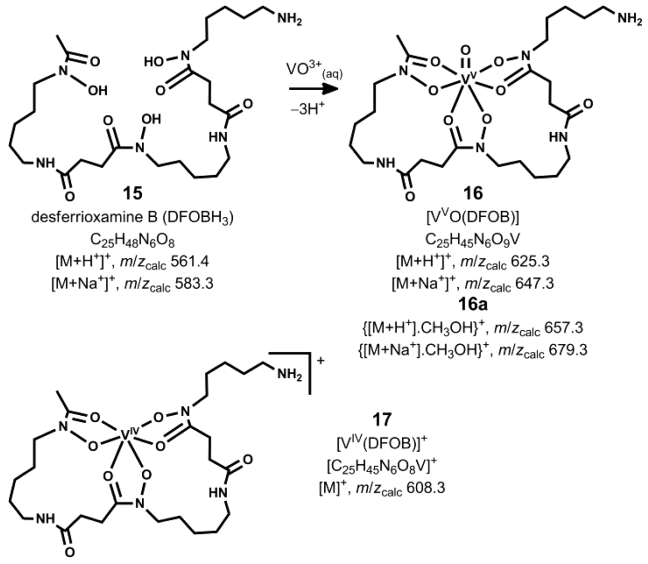

both solvents. Methanol did not act as a coordinating methoxide group toward six-coordinate **18** or seven-coordinate **19**.

The presence of six-coordinate V(V)/pbH$_2$ mononuclear complexes and six- and seven-coordinate V(V)/pbH$_2$ dinuclear complexes demonstrates that despite its restrained macrocyclic structure, there is sufficient conformational flexibility in the pbH$_2$ ligand to enable coordination from ancillary ligands. The steric and electronic influence of the *cis*-dioxido–Mo(VI) center, which is common to a number of Mo(VI)/hydroxamic acid complexes characterized by X-ray crystallography,[48,49] appeared to direct the compression of the pbH$_2$ macrocycle below the Mo(VI)-ligand plane to prevent binding of ancillary methanol-based ligands.

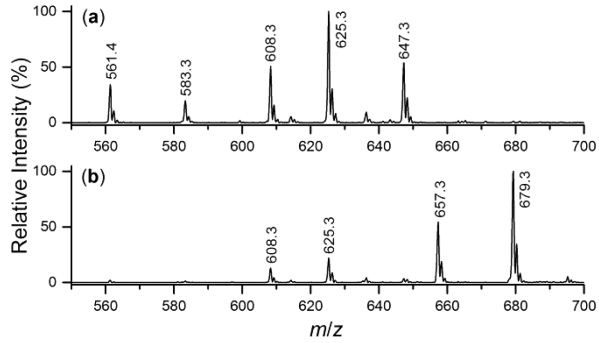

Figure 6. MS analysis (positive ion mode) from LC signals from solutions ([V(V)]/[DFOBH$_3$] = 1:1; pH ≈ 4) of V(V) and desferrioxamine B (DFOBH$_3$, **15**) in (a) H$_2$O or (b) H$_2$O/CH$_3$OH.

Table 2. LC-MS Data of Species Characterized from Solutions of V(V) and DFOBH$_3$ in H$_2$O or H$_2$O/CH$_3$OH

assignment	no	*m*/*z*$_{obs}$ (RI %)[a,b]	*m*/*z*$_{calc}$	ion
DFOBH$_3$	**15**	561.4 (34.2)	561.4	$[M + H^+]^+$
		583.3 (19.6)	583.3	$[M + Na^+]^+$
$[V^VO(DFOB)]$	**16**	625.3 (100)	625.3	$[M + H^+]^+$
		647.3 (53.7)	647.3	$[M + Na^+]^+$
$[V^VO(DFOB)]\cdot CH_3OH$	**16a**	657.3 (44.0)[c]	657.3	$[M + H^+]^+$
		679.3 (100)[c]	679.3	$[M + Na^+]^+$
$[V^{IV}(DFOB)]^+$	**17**	608.3 (50.7)	608.3	$[M]^+$

[a]RI, relative intensity. [b]RI values given for water system, unless specified otherwise. [c]Species observed only in methanol system.

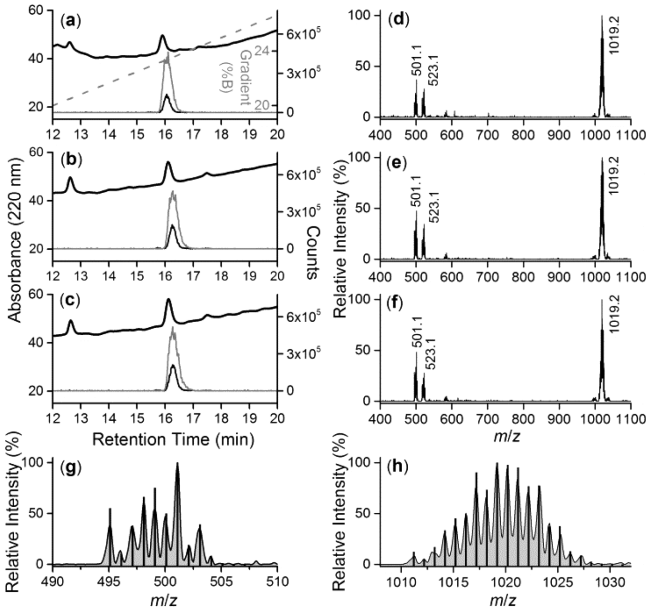

Figure 7. LC (a–c) and MS (d–f) traces from solutions of Mo(VI) and pbH$_2$ ([Mo(VI)]/[pbH$_2$] = 1:1; pH ≈ 4) in (a, d) H$_2$O; (b, e) H$_2$O/CH$_3$OH; or (c, f) H$_2$O/CD$_3$OD. LC detection used UV absorbance at 220 nm (black, heavy) and SIM counts at *m*/*z* 501 (black) and *m*/*z* 1019 (gray). The gradient (gray, broken) in (a) was the same in (b) and (c). The experimental (gray) and simulated (black) isotope patterns for $[Mo^{VI}(O)_2(pb)]$ ($[M + H^+]^+$, *m*/*z*$_{calc}$ 501.1) and $[(Mo^{VI}O(pb))_2(\mu\text{-}O)_2]$ ($[M + Na^+]^+$, *m*/*z*$_{calc}$ 1019.2) are shown in panels (g) and (h), respectively.

dx.doi.org/10.1021/ic500787v | *Inorg. Chem.* 2014, 53, 5852–5861

Table 3. LC-MS Data of Species Characterized From Solutions of Mo(VI) and pbH_2 in H_2O or H_2O/CH_3OH

assignment	no	m/z_{obs} (RI %)[a,b]	m/z_{calc}	ion
$[Mo^{VI}(O)_2(pb)]$	**18**	501.1 (37.0)	501.1	$[M + H^+]^+$
		523.1 (28.1)	523.1	$[M + Na^+]^+$
$[(Mo^{VI}O(pb))_2(\mu\text{-}O)_2]$	**19**	1019.2 (100)	1019.1	$[M + Na^+]^+$

[a]RI, relative intensity. [b]RI values given for water system, unless specified otherwise.

Chart 2. Species Characterized Using LC-MS from Solutions of Mo(VI) and pbH_2 in H_2O or H_2O/CH_3OH

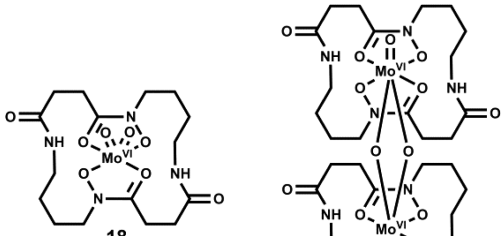

Since the concentrations of V(V) or Mo(VI) were relatively high compared to any trace amounts of Fe(III) that may have been present in the solvents, no signals in the pbH_2 or $DFOBH_3$ systems were ascribable to Fe(III) complexes (e.g., $[Fe(pb)]^+$; $[M]^+$, m/z_{calc} 426) (Supporting Information, Figure S5).[50,51] In the presence of a local source of mineralized or chelated iron in the ocean, it would be expected, based on high Fe(III)-siderophore affinity constants,[1−6] that Fe(III) would displace the V(V) or Mo(VI) coordinated to pbH_2 or any other marine siderophore. Studies of the mixed-ligand type siderophore azotobactin produced by *Azotobacter vinelandii* showed that there was a kinetic advantage in forming complexes with V(V) or Mo(VI) above Fe(III), with the latter element undergoing slow exchange when present in the form of insoluble Fe(III)−oxide/hydroxide complexes.[52]

CONCLUSION

This work sought to determine the phenomenon underlying the presence of two peaks in LC-MS measurements from solutions of V(V) and pbH_2 in H_2O/CH_3OH that were detected using a single SIM value at m/z 437 characteristic of $[V^VO(pb)]^+$. The data showed that the two peaks represented two populations of species with different ancillary ligands coordinated to the $[V^VO(pb)]^+$ core. Peak 1 contained $[V^VO(pb)]^+$ (**2**) in addition to $[V^VO(pb)(OH)]$ (**3**) and the (**2**)−(**3**) or (**3**)−(**3**) dinuclear products $[(V^VO(pb))_2(\mu\text{-}OH)]^+$ (**9**) or $[(V^VO(pb))_2(\mu\text{-}OH)_2]$ (**6**), respectively. Peak 2 contained $[V^VO(pb)]^+$ (**2**) in addition to $[V^VO(pb)(OCH_3)]$ (**4**) and the (**2**)−(**4**) or (**4**)−(**4**) dinuclear products $[(V^VO(pb))_2(\mu\text{-}OCH_3)]^+$ (**10**) or $[(V^VO(pb))_2(\mu\text{-}OCH_3)_2]$ (**7**), respectively. The order of elution of these groups of species was consistent with the trend in hydrophobicity of water and methanol (water < methanol). The SIM detection at m/z 437 for both peaks was a likely result of the presence of $[V^VO(pb)]^+$ as a dissociation product of $[(V^VO(pb))_2(\mu\text{-}OH)]^+$ (**9**) → $[V^VO(pb)]^+$ (**2**) + $[V^VO(pb)(OH)]$ (**3**)] (peak 1) and $[(V^VO(pb))_2(\mu\text{-}OCH_3)]^+$ (**10**) → $[V^VO(pb)]^+$ (**2**) + $[V^VO(pb)(OCH_3)]$ (**4**)] (peak 2).

The Mo(VI)/pbH_2 system gave fewer species in solution than the V(V)/pbH_2 system, with no evidence of methoxide coordination, most likely due to the steric and electronic effects of the *cis*-dioxido−$Mo(O)_2$ group. The fewer species in solution predicts for more favorable outcomes in Mo(VI)/pbH_2 crystallization trials, which are ongoing in our group.

The unequivocal assignment of dinuclear $[(V^VO(pb))_2(\mu\text{-}OCH_3)_2]$ (**7**) as the predominant species (100%) present in the V(V)/pbH_2 in H_2O/CH_3OH system was made upon the replacement of V_2O_5 with ^{50}V-enriched V_2O_5 as the V(V) source. This isotope enrichment gave rise to a distinct isotope pattern that was a composite of the three $^{51}V-^{51}V$, $^{51}V-^{50}V$, and $^{50}V-^{50}V$ species. The coordination of the methoxide ligand was confirmed upon the replacement of CH_3OH with CD_3OD, which formed $[(V^VO(pb))_2(\mu\text{-}OCD_3)_2]$ as the predominant species.

This work highlights the value of the use of isotopically enriched metal sources and deuterated solvents for the deconvolution of metal/siderophore speciation. The complexes identified in this work have relevance in the context of providing a better understanding of the speciation of siderophores excreted into the marine environment containing high concentrations of bioavailable V(V) and Mo(VI).

EXPERIMENTAL SECTION

Reagents and Chromatographic Resins. Bactopeptone and yeast extract were from Amyl media. Sea salt, hexadecyltrimethylammonium bromide (~99%), Chrome Azurol S (~65% dye), anhydrous piperazine (99%), 5-sulfosalicylic acid hydrate (95%), sodium chloride (≥99%), $Na_2MoO_4{\cdot}2H_2O$ (100%), desferrioxamine B·mesylate (>93%), and Chelex 100 resin were obtained from Sigma-Aldrich (St. Louis, MO, USA). $VOSO_4{\cdot}5H_2O$ (>96%) and V_2O_5 (>99%) were obtained from Merck (Darmstadt, Germany). ^{50}V-enriched V_2O_5 (^{50}V enrichment 36%) was from Oak Ridge National Laboratory (Oak Ridge, TN, USA). Chromatography was carried out using XAD-2 resin (Amberlite) and Ni(II) SepharoseTM 6 Fast Flow resin (GE Healthcare).

Instrumentation. Liquid chromatography-triple quadrupole mass spectrometry (LC/MS-QQQ) was conducted on an Agilent series 1200 LC system with Agilent 1290 Infinity binary pump with integrated vacuum degasser, autosampler, thermostated column compartment and diode array detector, and an Agilent 6400 series triple quadrupole mass spectrometer equipped with electrospray ionization (ESI) with Agilent Jet Stream technology. The injection volume was 5 μL, the capillary voltage was 3 kV, and the cone voltage was 25 V. The samples were analyzed on an Agilent C18 column (particle size 5 μm; 150 × 2.1 mm i.d.) with a gradient of 10−30% B over 27 min (A: 5% CH_3CN in 0.1% formic acid; B: 95% CH_3CN in 0.1% formic acid) at a flow rate of 0.2 mL min^{-1}. Agilent OpenLAB Chromatography Data System (CDS) ChemStation Edition was used for data acquisition and processing. Selected ion monitoring (SIM) was used at m/z values as specified.

Bacterial Cultures. *S. putrefaciens* ATCC 8071^T was obtained from the American Type Culture Collection (ATCC). Permanent stocks were maintained in Difco marine broth 2216 (Bacto) with 10% v/v dimethyl sulfoxide at −80 °C. Base medium contained bactopeptone (5 g L^{-1}), yeast extract (2 g L^{-1}), and sea salts (35 g L^{-1}) and was stirred with Chelex 100 resin (10−12 g L^{-1}) for 4 × 1.5 h. The pH

dx.doi.org/10.1021/ic500787v | Inorg. Chem. 2014, 53, 5852−5861

value of the decanted medium was adjusted to 7.00 ± 0.05 before sterilization with autoclaving (121 °C, 20 min). Plastic Erlenmeyer flasks were used for the cultures, and Milli-Q-grade H_2O was used throughout the culturing and purification procedures. Cultures of *S. putrefaciens* (100 mL in 500 mL flasks) were grown at room temperature in Fe-depleted medium containing 10 mM NaCl on a Ratek orbital shaker at 140 rpm for 6 d. The Chrome Azurol S (CAS) assay was used to monitor putrebactin production in liquid cultures.[53] An aliquot of the cell culture supernatant (100 μL) was mixed with CAS dye (100 μL), followed by the shuttle solution (4 μL). After 4 h, the absorbance of the solution was measured at 630 nm at 4 h using a SpectraMax M5 plate reader. Uninoculated medium was used as a control.

XAD-2 Chromatography. Siderophores were purified from culture supernatants with modifications to previous methods.[12,14,54−56]

At day 6 after inoculation, bacterial cells were pelleted by centrifugation, and the supernatant was loaded by gravity (flow rate = 5 mL min^{-1}) onto a column (30 × 2.5 cm i.d., column volume (CV) = 147 cm^3) containing XAD-2 resin. The resin had been prepared by batch washing in CH_3OH (1 CV) and H_2O (4 CV) before packing the column, and it was further equilibrated with H_2O after packing. After sample loading, the column was washed with H_2O (2 CV), 50% CH_3OH/H_2O (1.5 CV), and 100% CH_3OH (1.5 CV), and fractions of 20 mL were collected. For siderophore detection, an aliquot of sample (50 μL), H_2O (50 μL), CAS assay solution (100 μL), and shuttle solution (4 μL) were mixed in this order, and the absorbance value of the solution was measured at 630 nm after 4 h. The siderophore-positive fractions were eluted in the 50% CH_3OH/H_2O wash, and were pooled and dried in vacuo (external bath ∼38 °C).

Ni(II)-Based Immobilized Metal Ion Affinity Chromatography. The immobilized metal ion affinity chromatography (IMAC) column was prepared using a 20 mL bed volume of Ni(II) SepharoseTM 6 Fast Flow resin (GE Healthcare). The column was washed with Milli-Q water (5−10 CV) and equilibrated with binding buffer (10 mM HEPES, 0.2 M NaCl, pH 9.0; 5−10 CV). The semipurified siderophore residue was dissolved in binding buffer (∼5 mL) and was loaded onto the column. The column was washed with 5 CV of binding buffer, followed by 5−10 CV of elution buffer (10 mM HEPES, 0.2 M NaCl, pH 5.5), and fractions of 5 mL were collected. Siderophore-positive fractions, which eluted in the elution buffer wash, were lyophilized using a Labconco FreeZone freeze-dryer. To remove *N*-(2-hydroxyethyl)piperazine-*N*′-ethanesulfonic acid (HEPES) and NaCl, the dried sample was extracted in CH_3OH (∼1 mL), with insoluble materials removed by centrifugation (12 000 rpm, 5 min) using an Eppendorf centrifuge 5415R. The estimated yield of putrebactin (5.6 mg L^{-1}) was calculated using the CAS assay, with desferrioxamine B used as a reference compound. A multiplier was applied to correct for the trihydroxamic acid (standard) versus the dihydroxamic acid (target). There was evidence of impurities derived from culture medium (phenylalanine, tryptophan) at levels that did not perturb the V(V)/ or Mo(VI)/pbH_2 speciation.

Preparation of Solutions of V(V), V(IV), or Mo(VI) and Putrebactin for Analysis by LC-MS-QQQ. Stock solutions of metals were prepared by dissolving $VOSO_4{\cdot}5H_2O$ (0.0253 g, 0.1 mmol), V_2O_5 (0.0182 g, 0.1 mmol), or $Na_2MoO_4{\cdot}2H_2O$ (0.0242 g, 0.1 mmol) in 1 mL of H_2O to give final concentrations with respect to V(IV), V(V), or Mo(VI) of 100 mM, 200 mM, or 100 mM, respectively. An aliquot (100 μL) of the stock solution was added to 400 μL H_2O, and the pH value was adjusted with NaOH to pH 7 before the solution was made to a final volume of 1 mL with water to give a final concentration of 10 mM (V(IV) or Mo(VI)) or 20 mM (V(V)). A 10 mM solution of ^{50}V-enriched V_2O_5 was prepared by dissolving 0.9 mg of ^{50}V-enriched V_2O_5 in 0.5 mL of H_2O to give a solution of a concentration of 20 mM with respect to V(V). The V_2O_5 and ^{50}V-enriched V_2O_5 solutions were sonicated for 1 h.

The semipurified putrebactin extracts were lyophilized and redissolved in defined volumes of H_2O, CH_3OH, or CD_3OD to give solutions of a final concentration of ∼10 mM. Solutions of V(V) and pbH_2 were prepared from the addition of 10 μL of V(V) stock solution (20 mM) to 20 μL of pbH_2 stock solution (10 mM) to give a final solution of 6.6 mM V(V) and 6.6 mM pbH_2. The solutions of V(IV) and pbH_2 solutions were 3.3 mM V(IV) and 6.6 mM pbH_2. Solutions were incubated for 1−2 h and diluted to 1:50 in the relevant solvent (H_2O, H_2O/CH_3OH, or H_2O/CD_3OD) prior to analysis using LC-MS-QQQ. The pH values of stock solutions were adjusted to pH 7, and the pH value of the eluent of the LC-MS-QQQ system was pH ≈ 4, which was used as the final reported pH value in this study. The solutions of Mo(VI) and pbH_2 were 5 mM Mo(VI) and 5 mM pbH_2 and were analyzed after 24 h incubation as a 1:25 dilution. This sample was analyzed on LC-MS-QQQ with a gradient of 10−40% B over 36 min (A: 5% CH_3CN in 0.1% formic acid; B: 95% CH_3CN in 0.1% formic acid) at 220 nm. The DFOB stock (10 mM) was prepared by 1:10 dilution of 100 mM stock (0.0657 g in 1 mL of H_2O, pH 8). The solutions of V(V) and DFOB samples were prepared and analyzed using the same conditions as putrebactin.

Simulation of Mass Spectra. Mass spectra were simulated using ChemCalc.[37] Molecular formulas for the complexes formed in H_2O, CH_3OH, or CD_3OD between 36% ^{50}V-enriched V_2O_5 and pbH_2 used the syntax: $V\{64,36\}_aC_xH_yD_zN_uO_vNa_w$ (a = 1, mononuclear; a = 2, dinuclear; x, y, z, u, v, w = various); or between theoretical 100% $^{50}V_2O_5$ and pbH_2: $[50\ V]_aC_xH_yD_zN_uO_vNa_w$ (a, x, y, z, u, v, w, as above).

■ ASSOCIATED CONTENT

Supporting Information

Additional data: pbH_2 purity (Figure S1), MS traces from solutions of V(V) or V(IV) and pbH_2 (Figure S2), MS simulations of species in main paper (Table S1), MS simulations of species not in main paper (Figure S3), ESI-MS traces from solutions of V(V) and pbH_2 as a function of time (Figure S4), and measurements of $[Fe(pb)]^+$ in solutions of V(V) or Mo(VI) and pbH_2 that could potentially form from the presence of trace Fe(III) in solvents (Figure S5). This material is available free of charge via the Internet at http://pubs.acs.org.

■ AUTHOR INFORMATION

Corresponding Author

*E-mail: rachel.codd@sydney.edu.au.

Notes

The authors declare no competing financial interest.

■ ACKNOWLEDGMENTS

The Australian Research Council is acknowledged for research funding (R.C.). The University of Sydney is acknowledged for the award of cofunded postgraduate scholarships to C.Z.S. and A.A.H.P.

■ REFERENCES

(1) Neilands, J. B. *J. Biol. Chem.* **1995**, *270*, 26723−26726.
(2) Sandy, M.; Butler, A. *Chem. Rev.* **2009**, *109*, 4580−4595.
(3) Hider, R. C.; Kong, X. *Nat. Prod. Rep.* **2010**, *27*, 637−657.
(4) Butler, A.; Theisen, R. M. *Coord. Chem. Rev.* **2010**, *254*, 288−296.
(5) Budzikiewicz, H. In *Progress in the Chemistry of Organic Natural Products;* Kinghorn, A. D., Falk, H., Kobayashi, J., Eds.; Springer-Verlag: New York, 2010; Vol. *92*, p 1−75.
(6) Crumbliss, A. L.; Harrington, J. M. *Adv. Inorg. Chem.* **2009**, *61*, 179−250.
(7) Faraldo-Gómez, J.; Sansom, M. S. P. *Nat. Rev. Mol. Cell. Biol.* **2003**, *4*, 105−116.
(8) Miethke, M. *Metallomics* **2013**, *5*, 15−28.
(9) Ratledge, C.; Dover, L. G. *Annu. Rev. Microbiol.* **2000**, *54*, 881−941.
(10) Shanzer, A.; Felder, C. E.; Barda, Y. In *The Chemistry of Hydroxylamines, Oximes and Hydroxamic Acids;* Rappoport, Z.,

Liebman, J. F., Eds.; John Wiley & Sons, Ltd.: Chichester, Engalnd, 2009; p 751−815.
(11) Mawji, E.; Gledhill, M.; Milton, J. A.; Tarran, G. A.; Ussher, S.; Thompson, A.; Wolff, G. A.; Worsfold, P. J.; Achterberg, E. P. *Environ. Sci. Technol.* **2008**, *42*, 8675−8680.
(12) Ledyard, K. M.; Butler, A. *J. Biol. Inorg. Chem.* **1997**, *2*, 93−97.
(13) Nishio, T.; Tanaka, N.; Hiratake, J.; Katsube, Y.; Ishida, Y.; Oda, J. *J. Am. Chem. Soc.* **1988**, *110*, 8733−8734.
(14) Soe, C. Z.; Codd, R. *ACS Chem. Biol.* **2014**, *9*, 945−956.
(15) Codd, R. *Coord. Chem. Rev.* **2008**, *252*, 1387−1408.
(16) Schalk, I. J.; Hannauer, M.; Braud, A. *Environ. Microbiol.* **2011**, *13*, 2844−2854.
(17) Gez, S.; Luxenhofer, R.; Levina, A.; Codd, R.; Lay, P. A. *Inorg. Chem.* **2005**, *44*, 2934−2943.
(18) Chatterjee, B. *Coord. Chem. Rev.* **1978**, *26*, 281−303.
(19) Marmion, C. J.; Griffith, D.; Nolan, K. B. *Eur. J. Inorg. Chem.* **2004**, 3003−3016.
(20) Möllmann, U.; Heinisch, L.; Bauernfeind, A.; Köhler, T.; Ankel-Fuchs, D. *BioMetals* **2009**, *22*, 615−624.
(21) Roosenberg, J. M. I.; Lin, Y.-M.; Lu, Y.; Miller, M. J. *Curr. Med. Chem.* **2000**, *7*, 159−197.
(22) Chu, B. C.; Garcia-Herreno, A.; Johanson, T. H.; Krewulak, K. D.; Lau, C. K.; Sean Peacock, R.; Slavinskaya, Z.; Vogel, H. J. *BioMetals* **2010**, *23*, 601−611.
(23) Wencewicz, T. A.; Moellmann, U.; Long, T. E.; Miller, M. J. *BioMetals* **2009**, *22*, 633−648.
(24) Liu, J.; Obando, D.; Schipanski, L. G.; Groebler, L. K.; Witting, P. K.; Kalinowski, D. S.; Richardson, D. R.; Codd, R. *J. Med. Chem.* **2010**, *53*, 1370−1382.
(25) Liddell, J. R.; Obando, D.; Liu, J.; Ganio, G.; Volitakis, I.; Mok, S. S.; Crouch, P. J.; White, A. R.; Codd, R. *Free Radical Biol. Med.* **2013**, *60*, 147−156.
(26) Mislin, G. L. A.; Schalk, I. J. *Metallomics* **2014**, *6*, 408−420.
(27) Rehder, D. *Dalton Trans.* **2013**, *42*, 11749−11761.
(28) Emerson, S. R.; Huested, S. S. *Mar. Chem.* **1991**, *34*, 177−196.
(29) Butler, A. *Science* **1998**, *281*, 207−210.
(30) Pakchung, A. A. H.; Soe, C. Z.; Lifa, T.; Codd, R. *Inorg. Chem.* **2011**, *50*, 5978−5989.
(31) Fisher, D. C.; Barclay-Peet, S. J.; Balfe, C. A.; Raymond, K. N. *Inorg. Chem.* **1989**, *28*, 4399−4406.
(32) Bell, J. H.; Pratt, R. F. *Inorg. Chem.* **2002**, *41*, 2747−2753.
(33) Spasojevic, I.; Boukhalfa, H.; Stevens, R. D.; Crumbliss, A. L. *Inorg. Chem.* **2001**, *40*, 49−58.
(34) Caudle, M. T.; Stevens, R. D.; Crumbliss, A. L. *Inorg. Chem.* **1994**, *33*, 6111−6115.
(35) Haratake, M.; Fukunaga, M.; Ono, M.; Nakayama, M. *J. Biol. Inorg. Chem.* **2005**, *10*, 250−258.
(36) Sutradhar, M.; Kirillova, M. V.; Guedes da Silva, M. M. C.; Martins, L. M. D. R. S.; Pombeiro, A. J. L. *Inorg. Chem.* **2012**, *51*, 11229−11231.
(37) Patiny, L.; Borel, A. *J. Chem. Inf. Model.* **2013**, *53*, 1223−1228.
(38) Colton, R.; D'Agostino, A.; Traeger, J. C. *Mass Spectrom. Rev.* **1995**, *14*, 79−106.
(39) Di Marco, V. B.; Bombi, G. G.; Zambon, S.; Traldi, P. *J. Mass Spectrom.* **2009**, *44*, 120−127.
(40) Di Marco, V. B.; Bombi, G. G. *Mass Spectrom. Rev.* **2006**, *25*, 347−379.
(41) Bakhtiar, R.; Hop, C. E. C. A. *J. Phys. Org. Chem.* **1999**, *12*, 511−527.
(42) Patra, S.; Chatterjee, S.; Si, T. K.; Mukherjea, K. K. *Dalton Trans.* **2013**, *42*, 13425−13435.
(43) Crans, D. C. In *Metal Ions in Biological Systems;* Sigel, H., Sigel, A., Eds.; Marcel Dekker: New York, 1995; Vol. *31*, p 147−209.
(44) Gibney, B. R.; Stemmler, A. J.; Pilotek, S.; Kampf, J. W.; Pecoraro, V. L. *Inorg. Chem.* **1993**, *32*, 6008−6015.
(45) Karpishin, T. B.; Dewey, T. M.; Raymond, K. N. *J. Am. Chem. Soc.* **1993**, *115*, 1842−1851.
(46) Luterotti, S.; Grdinic, V. *Analyst* **1986**, *111*, 1163−1165.
(47) Howarth, R. W.; Cole, J. J. *Science* **1985**, *229*, 653−655.
(48) Brown, D. A.; Bögge, H.; Coogan, R.; Doocey, D.; Kemp, T. J.; Müller, A.; Neumann, B. *Inorg. Chem.* **1996**, *35*, 1674−1679.
(49) Brewer, G. A.; Sinn, E. *Inorg. Chem.* **1981**, *20*, 1823−1830.
(50) Gledhill, M. *Analyst* **2001**, *126*, 1359−1362.
(51) McCormack, P.; Worsfold, P. J.; Gledhill, M. *Anal. Chem.* **2003**, *75*, 2647−2652.
(52) Wichard, T.; Bellenger, J.-P.; Morel, F. M. M.; Kraepiel, A. M. L. *Environ. Sci. Technol.* **2009**, *43*, 7218−7224.
(53) Schwyn, B.; Neilands, J. B. *Anal. Biochem.* **1987**, *160*, 47−56.
(54) Pakchung, A. A. H.; Soe, C. Z.; Codd, R. *Chem. Biodiversity* **2008**, *5*, 2113−2123.
(55) Soe, C. Z.; Pakchung, A. A. H.; Codd, R. *Chem. Biodiversity* **2012**, *9*, 1880−1890.
(56) Braich, N.; Codd, R. *Analyst* **2008**, *133*, 877−880.